

## Design of Dual-Band Bandpass Filter with Closely Spaced Passbands and Multiple Transmission Zeros

Yang Xiong<sup>1</sup>, Li Tian Wang<sup>1</sup>, Wei Zhang<sup>1</sup>, Fan Zhang<sup>1</sup>,  
Doudou Pang<sup>1</sup>, Ming He<sup>1, 2, \*</sup>, Xinjie Zhao<sup>1</sup>, and Lu Ji<sup>1</sup>

**Abstract**—Two compact dual-band bandpass filters (BPFs) with closely spaced passbands are presented in this paper. Each of the filters consists of a stub loaded resonator, to which shorted lines are coupled. The ratio of the center frequencies of two passbands can be easily adjusted from 1.2 to 1.1 by changing the gap of the coupled line. In addition, seven transmission zeros (TZs) can be yielded to obtain high passband selectivity and enhance the out of band performances. As an example, two filters are designed, fabricated and measured. Both filters exhibit the merits of high passband selectivity, very low center frequency ratio, and wide stopband suppression.

### 1. INTRODUCTION

To fulfill the requirement of multi-service in modern communication systems, much attention has been paid to exploiting dual-band BPF with merits of compact circuit size, wide stopband, high selectivity, etc. As a straightforward method, dual-band BPFs can be easily designed by combining several individual multiple-mode resonators (MMR) or BPFs with appropriate arrangement [1–5]. Obviously, the center frequency ratio is controllable naturally in this method, but it involves changing and optimizing a large number of dimensional parameters. Thus, it is difficult to adjust the center frequency ratio effectively. Plus, the drawback of large circuit area is also obvious. To overcome the flaws of overlarge circuit size and improve the out of band performances, defected ground structure (DGS) has been widely applied in dual-band BPFs design [6–8]. In this method, DGS provides an extra degree of freedom to control the resonant frequencies by properly alternating the shape or its size at the expense of backside fabrication process. Besides, owing to the merits of simple structure and easy regulation, MMR is a promising candidate for multi-band design [9–11]. Although the filters have fully demonstrated their merits, the filters [1, 3, 4, 7–11] are not suitable for channel selection in wireless communication systems, because most of the reported dual-band BPFs using MMR possess a high center frequency ratio. Recently, there are a few attempts on very closely spaced dual-band BPF with adjustable center frequency ratio using a single MMR.

In this paper, two compact dual-band BPFs with very low center frequency ratio are presented. Each of the filters consists of a stub loaded resonator, and two shorted lines are coupled to the stub loaded resonator. The classic method of even- and odd-mode analysis technique is adopted to interpret the resonant properties of this MMR. In addition, seven TZs are yielded to obtain high passband selectivity and improve the out of band performances. In lower stopband, over 30 dB suppression is obtained from DC to 3.47 GHz. In upper stopband, 22 dB suppression ranges from 4.54 GHz to 9.66 GHz. For demonstration, two filters are designed, fabricated, and tested.

---

*Received 28 June 2017, Accepted 8 August 2017, Scheduled 31 August 2017*

\* Corresponding author: Ming He (heming@nankai.edu.cn).

<sup>1</sup> College of Electronic Information and Optical Engineering, Nankai University, Tongyan Road No. 38, Jinnan District, Tianjin 300350, China. <sup>2</sup> Tianjin Key Laboratory of Optoelectronic Sensor and Sensing Network Technology, Tongyan Road No. 38, Jinnan District, Tianjin 300350, China.

## 2. DUAL-BAND BPF DESIGN AND ANALYSIS

The ideal transmission line model (TLM) and physical layout of the proposed MMR are sketched in Figs. 1(a) and 1(b), respectively. We use the classic method of even- and odd-mode analysis technique to explain the resonant properties of the MMR for its property of symmetry. The equivalent even- and odd-mode circuits are illustrated in Figs. 1(c) and 1(d).

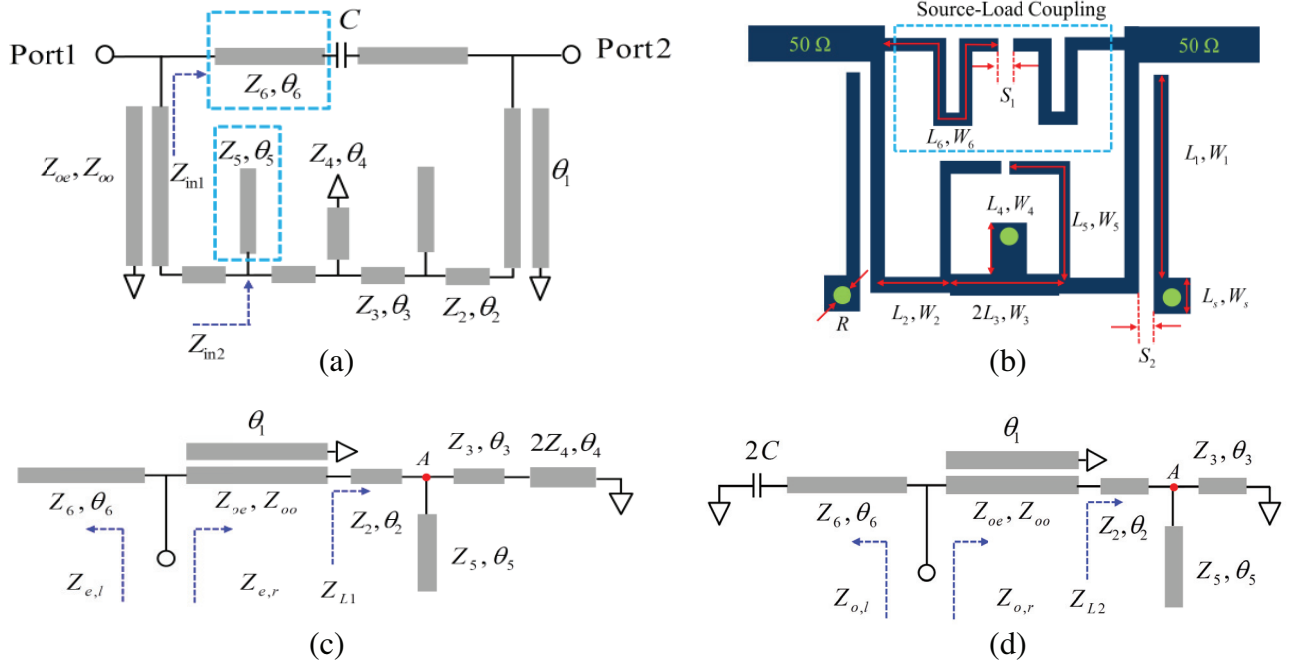


**Figure 1.** (a) TLM, (b) physical layout of the proposed MMR, (c) even-mode equivalent circuit and (d) odd-mode equivalent circuit.

As an example, the parameters are set as follows:  $Z_{0e} = 175$ ,  $Z_{0o} = 90$ ,  $Z_2 = 74$ ,  $Z_3 = 106$ ,  $Z_4 = 80$ ,  $Z_5 = Z_6 = 106$ ,  $\theta_1 = 90^\circ$ ,  $\theta_2 = \theta_3 = 19^\circ$ ,  $\theta_4 = 3.3^\circ$ ,  $\theta_5 = 60^\circ$ ,  $\theta_6 = 138^\circ$  and  $f_0 = 4$  GHz (reference frequency for electrical length calculation). The frequency response of  $S$ -parameter and  $\text{Im}(Y_{in})$  are simulated using TLM, which are shown in Figs. 2(a) and 2(b), respectively. It can be found that four transmission poles (TPs) are excited when  $\text{Im}(Y_{in}) = 0$ .

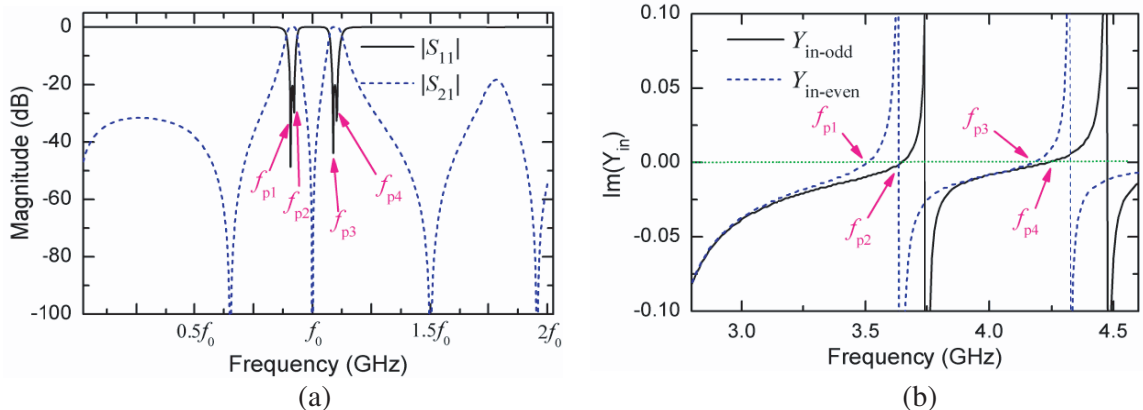


**Figure 2.** Simulated frequency response of (a)  $S$ -parameter, and (b)  $\text{Im}(Y_{in})$ .

According to transmission line theory and transverse resonant conditions, we have

$$\text{Im}(Y_{e,l} + Y_{e,r}) = 0 \quad (1)$$

$$\text{Im}(Y_{o,l} + Y_{o,r}) = 0 \quad (2)$$

where  $Y_{e,l}$  and  $Y_{e,r}$  denote the input admittances from the left side and right side of the reference plane when even-mode is excited. Likewise,  $Y_{o,l}$  and  $Y_{o,r}$  represent the input admittances from the left side and right side of the reference plane when odd-mode is excited.

For even-mode excitation,

$$Y_{e,l} = jY_6 \tan \theta_6 \quad (3)$$

To derive  $Y_{e,r}$ , we have to calculate the matrix of  $[Z]$  of the shorted coupled line [12]:

$$[Z] = \begin{bmatrix} Z_{11} & Z_{12} \\ Z_{21} & Z_{22} \end{bmatrix} \quad (4)$$

$$Z_{22} = j \frac{2Z_{0e}Z_{0o}(\tan(\theta_1/2) - \csc \theta_1)}{Z_{0e} + Z_{0o}} \quad (5)$$

$$Z_{12} = Z_{21} = -j \frac{2Z_{0e}Z_{0o} \csc \theta_1}{Z_{0e} + Z_{0o}} \quad (6)$$

$$Z_{11} = j \frac{(Z_{0e} - Z_{0o})^2 \tan \theta_1}{2(Z_{0e} + Z_{0o})} + Z_{22} \quad (7)$$

By transforming the matrix of  $[Z]$  to  $\begin{bmatrix} A & B \\ C & D \end{bmatrix}$ , the input impedance  $Z_{e,r}$  can be given as

$$Z_{e,r} = \frac{AZ_{L1} + B}{CZ_{L1} + D} \quad (8)$$

As shown in Fig. 1(c),  $Y_{L1}$  ( $1/Z_{L1}$ ) can be easily calculated as:

$$Y_{L1} = Y_2 \frac{Y_{inA} + jY_2 \tan \theta_2}{Y_2 + jY_{inA} \tan \theta_2} \quad (9)$$

$$Y_{inA} = jY_3 \frac{2Y_3 \tan \theta_3 - Y_4 \cot \theta_4}{2Y_3 + Y_4 \tan \theta_3 \cot \theta_4} + jY_5 \tan \theta_5 \quad (10)$$

Therefore, the even-mode resonant frequencies  $f_{p1}$  and  $f_{p3}$  can be solved based on the mentioned above equations to find its real roots using numerical calculation. In the method of numerical calculation, the initial values of the electrical lengths are calculated at  $f_0$ . And all of the electrical lengths should be recalculated as  $\theta'_n = \theta_n f_i / f_0$  ( $n = 1, 2, 3$ ) when the frequency  $f_i$  is considered. Then, we substitute the updated values into Equation (3)–(10). If Equation (1) is satisfied, it means that  $f_{e1} = f_i$  is the one even-mode resonant frequency that we are searching for. The odd-mode resonant frequencies can be solved by the same process. The resonant properties versus varied  $\theta_2$ ,  $\theta_3$ ,  $\theta_4$  and  $\theta_5$  are illustrated in Fig. 3. There are four TPs in two groups, and each group has two poles and is close to the center frequency  $f_0$ . It can be observed from Fig. 3(a) that  $\theta_2$  mainly affects the first group resonant modes with slightly variation in second group. It is found that  $\theta_3$  mainly impacts on  $f_{p1}$  and  $f_{p2}$  when smaller  $\theta_3$  is not considered. As can be seen,  $f_{p1}$  and  $f_{p3}$  will shift down when  $\theta_4$  gets large, whereas  $f_{p2}$  and  $f_{p4}$  keep unchanged. It can be observed from Fig. 3(d) that  $f_{p1}$ ,  $f_{p2}$ ,  $f_{p3}$  and  $f_{p4}$  decrease with the increase of  $\theta_5$ .

As shown in Fig. 4, we investigate the frequency responses of  $|S_{21}|$  and  $Z_{in}$  using TLM. It can be seen if  $Z_{in} = 0$  is satisfied at a certain frequency, a TZ will be generated at this frequency, which is attributed to the introduction of virtual ground to short out the transmission signal, as shown in Fig. 1(a). Thus we can derive the following equations:

$$Z_{in1} = -jZ_6 \cot(\theta_6) = 0 \quad (11)$$

$$Z_{in2} = -jZ_5 \cot(\theta_5) = 0 \quad (12)$$

$$f_{t1} = (2n + 1)\pi f_0 / 2\theta_6, \quad (n = 0, 1, 2 \dots) \quad (13)$$

$$f_{t2} = (2n + 1)\pi f_0 / 2\theta_5, \quad (n = 0, 1, 2 \dots) \quad (14)$$

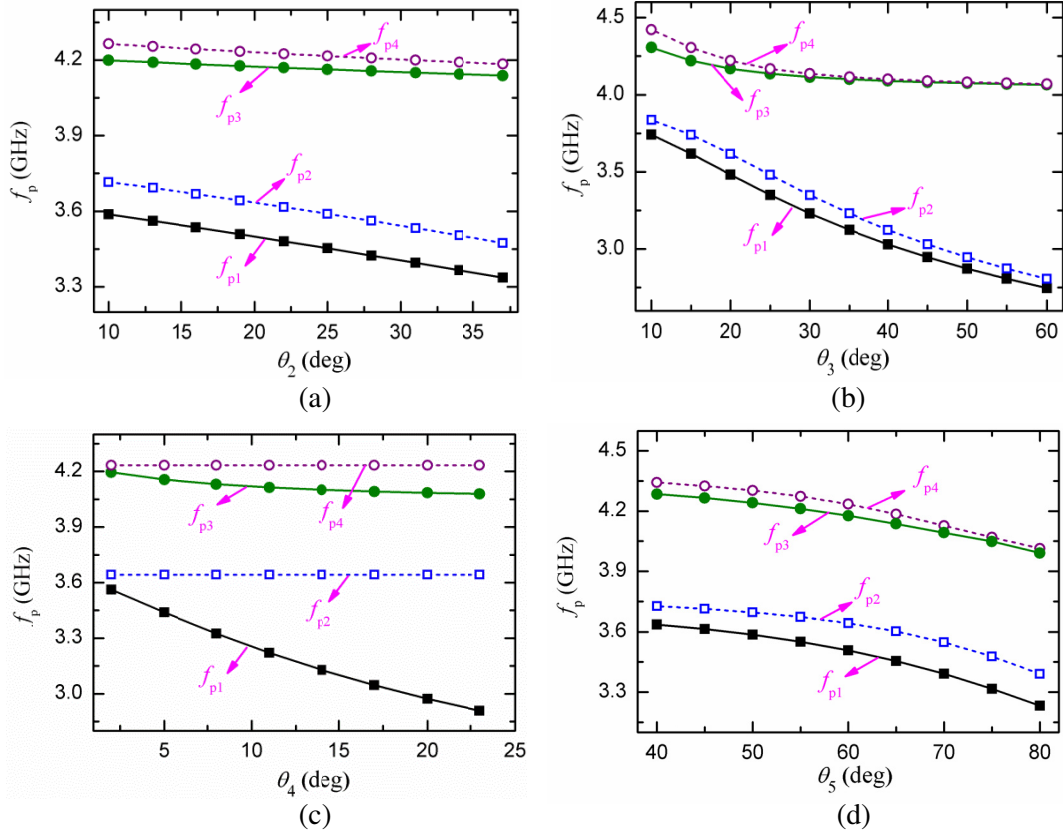


**Figure 3.** Resonant frequencies versus (a)  $\theta_2$ , (b)  $\theta_3$ , (c)  $\theta_4$ , and (d)  $\theta_5$ .

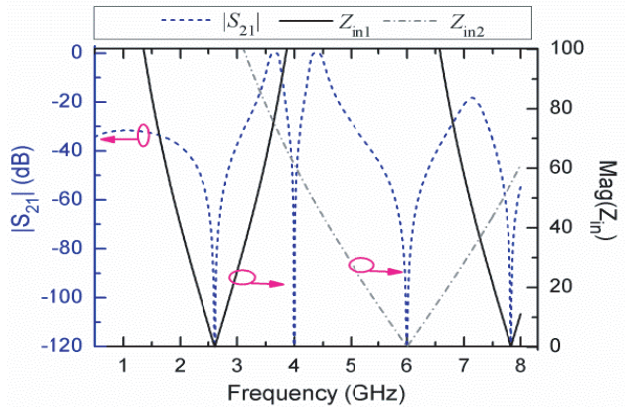


**Figure 4.** Frequency responses of  $|S_{21}|$  and  $Z_{in}$ .

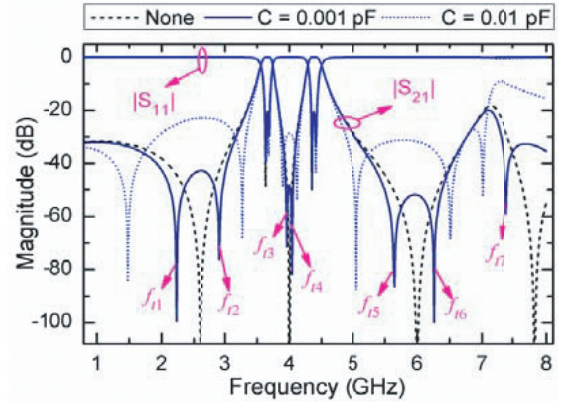


**Figure 5.** Frequency responses versus varied source-load coupling strength.

The TZ located at  $f_0$  is generated by  $Z_{in} = \infty$  at input port, thus it blocks the signals transmitted from port 1 to port 2, which results in the introduction of TZ. To improve the performances of the out of band, we use the capacitive coupling between input port and output port, as shown in Fig. 1(b). The frequency responses versus varied source-load coupling strength are shown in Fig. 5, in which the capacitor  $C$  represents the source-load coupling. It can be found that more TZs are generated when capacitive coupling is introduced.

As illustrated in Fig. 6(a), the frequency responses of  $S$ -parameter with varied  $S_2$  are simulated

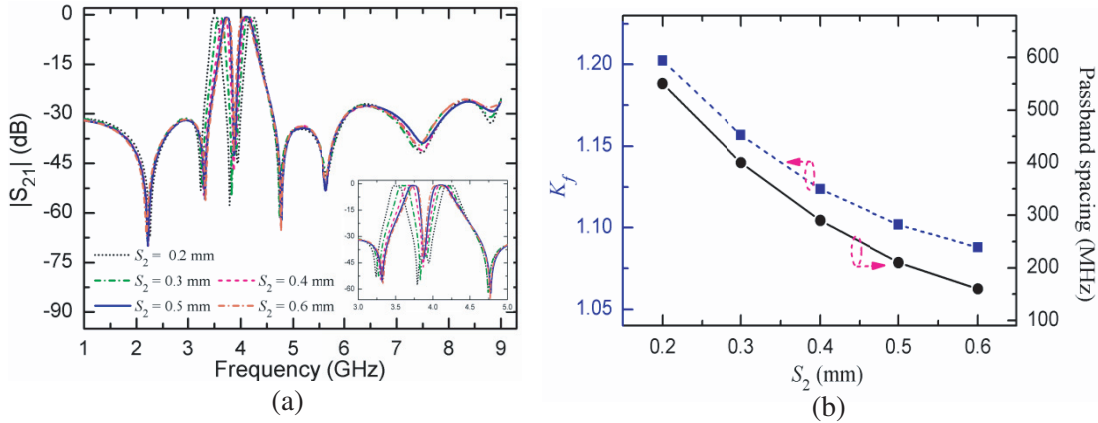


**Figure 6.** (a) The frequency response of  $|S_{21}|$  versus varied  $S_2$ , (b)  $K_f$  and passband spacing versus varied  $S_2$ .

using full-wave electromagnetic simulator. Passband spacing and  $K_f$  (the ratio of the center frequencies of two passbands) are extracted from the simulation results, which are record in Fig. 6(b). As can be seen, the passband spacing and  $K_f$  decrease with the increase of  $S_2$ . It can also be found that the parameter of  $S_2$  mainly impacts on the center frequencies of the two passband, whereas the out of band performances keep almost unchanged. So, we can easily adjust  $K_f$  by changing  $S_2$  with all the rest of parameters remaining unchanged.

### 3. FILTERS IMPLEMENT AND MEASURED RESULTS

In this work, a substrate of Rogers 4003c with parameters of  $\epsilon_r = 3.38$ ,  $h = 0.508$  mm and  $\tan \delta = 0.0027$  is chosen to implement the filters. The geometrical dimension parameters of filter A are given as follows (unit: mm):  $L_1 = 11.5$ ,  $L_2 = 4$ ,  $L_3 = 2.5$ ,  $L_4 = 0.95$ ,  $L_5 = 9.5$ ,  $L_6 = 17.4$ ,  $L_S = 0.95$ ,  $W_1 = W_2 = 0.2$ ,  $W_3 = 0.4$ ,  $W_4 = 0.9$ ,  $W_5 = W_6 = 0.2$ ,  $W_s = 0.6$ ,  $R = 0.4$ ,  $S_1 = S_2 = 0.4$ . The only difference between filter B and filter A is  $S_2$ , which is set at 0.6 mm in filter B. Both filters A and B are compact with overall size approximately  $15.4\text{ mm} \times 13.5\text{ mm}$  (excluding the feed lines), which corresponds to  $0.32\lambda_g \times 0.28\lambda_g$ , where  $\lambda_g$  is the guided wavelength at 3.81 GHz. For filter A, the measured frequency responses are characterized using Agilent E5071C vector network analyzer, whereas filter B is tested by Anritsu vector network analyzer. Fig. 7 plots the simulated and measured results of filter A and filter B. It can be observed from Fig. 7(a) that the return losses of the two passbands are better than 28.8 dB and 20.3 dB, and the measured  $f_{c1}$  and  $f_{c2}$  centered at 3.73 GHz and 4.29 GHz with 3-dB fractional

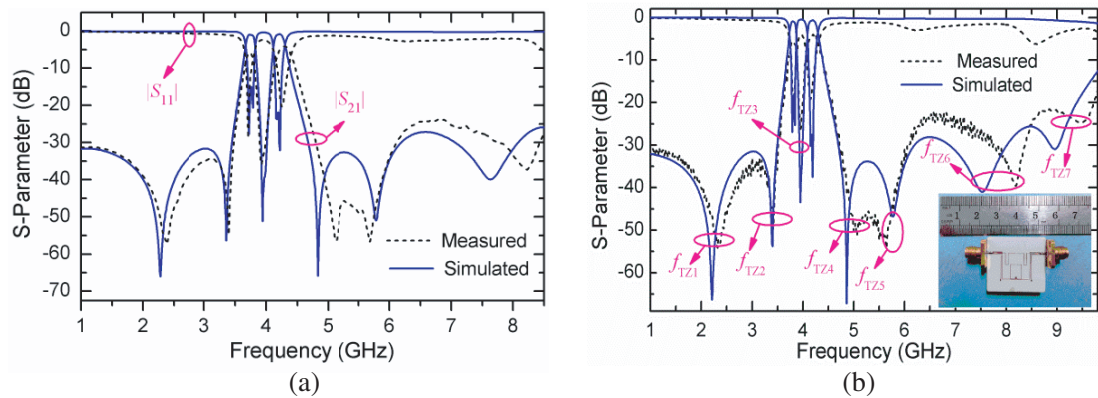


**Figure 7.** Simulated and measured results of (a) filter A and (b) filter B.

bandwidths (FBWs) of 3.7% and 5.7%, respectively. For filter B, the return losses are 24 dB/19.2 dB, and the measured  $f_{c1}$  and  $f_{c2}$  centered at 3.81 GHz and 4.2 GHz with 3-dB FBWs of 3.2% and 5.7%, respectively. In addition, multiple TZs are generated in out of band, which brings wide stopband suppression with 30 dB in lower stopband and 20 dB in upper stopband. The band-to-band isolations of filter A and filter B are 35.9 dB and 26.3 dB, respectively. Table 1 gives a performance comparison between this work and some other published works. It can be seen that the proposed dual-band BPFs possess the merits of low  $K_f$ , wide stopband suppression, high band-to-band isolation, etc.

**Table 1.** Comparison with some published works.

Ref.	$K_f$	TZs	FBW (%)	Easy to adjust $K_f$	Size ( $\lambda_g \times \lambda_g$ )
[2]	1.15	4	7.8/7.2	×	$0.24 \times 0.23$
[3]	1.46	6	9.6/7.7	×	$0.27 \times 0.18$
[6]	1.3	4	17/8.4	✓	$0.69 \times 0.38$
[9]	1.59	4	9.6/12	×	$0.14 \times 0.09$
Filter B	1.1	7	3.2/5.7	✓	$0.32 \times 0.28$

#### 4. CONCLUSION

In this paper, two compact dual-band BPFs with closely spaced passbands and multiple transmission zeros are presented. The  $K_f$  can be easily adjusted by changing the parameter of  $S_2$ . The resonant properties of the filters and the mechanism of generating TZs are discussed. The proposed dual-band BPFs have very low  $K_f$ , wide stopband suppression, high passband selectivity, etc. These merits make the proposed filters attractive for channel selection in wireless communication systems.

#### ACKNOWLEDGMENT

This work was supported by the Tianjin Research Program of Application Foundation and Advanced Technology (15JCQNJC01300).

#### REFERENCES

- Chen, W. Y., M. H. Weng, S. J. Chang, and H. Kuan, "A high selectivity dual-band filter using ring-like SIR with embedded coupled open stubs resonators," *Journal of Electromagnetic Waves and Applications*, Vol. 25, Nos. 14–15, 2011–2021, 2011.
- Liu, S., J. Xu, and Z. T. Xu, "Compact dual-band bandpass filters using complementary split-ring resonators with closely spaced passbands," *Electronics Letters*, Vol. 52, No. 15, 1312–1314, 2016.
- Eun, J. W. and J. H. Lee, "A microstrip dual-band bandpass filter using feed line with SIR," *IEICE Electronics Express*, Vol. 14, No. 4, 1–7, 2017.
- Denis, B., K. J. Song, and F. Zhang, "Compact dual-band bandpass filter using open stub-loaded stepped impedance resonator with cross-slots," *International Journal of Microwave and Wireless Technologies*, Vol. 9, No. 2, 269–274, 2016.
- Belyaev, B. A., A. M. Serzhantov, and V. V. Tyurnev, "A miniature dual-band filter based on microstrip dual-mode resonators," *Technical Physics Letters*, Vol. 38, No. 9, 839–842, 2012.
- Chen, D., L. Zhu, and C. H. Cheng, "A novel dual-band bandpass filter with closely spaced passbands," *IEEE Microwave and Wireless Components Letters*, Vol. 24, No. 1, 38–40, 2014.
- Wu, B., C. H. Liang, P. Y. Qin, and Q. Li, "Compact dual-band filter using defected stepped impedance resonator," *IEEE Microwave and Wireless Components Letters*, Vol. 18, No. 10, 674–676, 2008.

8. Song, K. J., F. Zhang, and Y. Fan, "Miniaturized dual-band bandpass filter with good frequency selectivity using SIR and DGS," *AEU-International Journal of Electronics and Communications*, Vol. 68, No. 5, 384–387, 2014.
9. Sun, S. J., T. Su, K. Deng, B. Wu, and C. H. Liang, "Compact microstrip dual-band bandpass filter using a novel stub-loaded quad-mode resonator," *IEEE Microwave and Wireless Components Letters*, Vol. 23, No. 9, 465–467, 2014.
10. Liu, H. W., B. P. Ren, X. H. Guan, J. H. Lei, and S. Li, "Compact dual-band bandpass filter using quadruple-mode square ring loaded resonator (SRLR)," *IEEE Microwave and Wireless Components Letters*, Vol. 23, No. 4, 181–183, 2014.
11. Xu, J., W. Wu, and C. Miao, "Compact and sharp skirts microstrip dual-mode dual-band bandpass filter using a single quadruple-mode resonator (QMR)," *IEEE Transactions on Microwave Theory and Techniques*, Vol. 61, No. 3, 1104–1113, 2013.
12. Matthaei, G., L. Young, and E. M. T. Jones, *Microwave Filters Impedance-Matching Networks, and Coupling Structures*, McGraw-Hill, New York, 1964.